TITLE

Marat Musin [1] [2], Jiasheng Huang [1], Haojing Yan [2],
Draft version May 20, 2019

ABSTRACT

Keywords: infrared: galaxies — submillimeter: galaxies — galaxies: starburst — methods: data analysis

1. INTRODUCTION

1.1. *Lilly-Madau formalism*

1.2. *SED fitting as a standard technique of mass and redshift estimation*

SED fitting is now a standard technique of deriving stellar mass and photometric redshifts for a large set of galaxies. In this method multi-band photometry for a given galaxy is fitted to a series of a templates predicted by a certain stellar population synthesis (SPS) model. The best-fit template gives the parameters of the galaxy, including its redshift and mass. Historically, SPS models were using restframe optical photometry. One caveat is the degeneracy between the dust extinction and age of the stellar population, as both make the color of galaxy red, i.e. galaxy can be red because it is intrinsically red with no young massive star and ongoing star-formation, or it can be very dusty, or it can be metal-rich and metals effectively absorb light in the bluer bands. Solution to this is to implement restframe near-IR where light suffers much less extinction (comparing to restframe UV and optical) and thus the degeneracy can be broken. We aim to build the largest sample of galaxies with optical and near-IR photometry over a large sky area. The natural choice for us then is to use optical Sloan Digital Sky Survey (SDSS) and IR all-sky data from Wide-Field Infrared Survey Explorer (WISE).

1.3. *problems associated with construction of the catalog*

Blending, poor spatial resolution in IR our method – template fitting

1.4. *Goal of this paper*

In this paper we present our technique for construction a catalog of galaxies with reliable SED data in optical and near-IR in Stripe 82 field. We discuss data selection, sources identification in different bands and problems associated with it.

2. DATA DESCRIPTION

2.1. *SDSS and Stripe 82*

The imaging component of the SDSS, which was done in five broad bands ($u'g'r'i'z'$), has covered 14,555 deg^2. In most area, the SDSS only scanned for one pass at

[1] Chinese Academy of Sciences South America Center for Astronomy (CASSACA), National Astronomical Observatories, Chinese Academy of Sciences, Beijing 100012, China
[2] Department of Physics & Astronomy, University of Missouri, Columbia, MO 65211, USA

an exposure time of 53.9 seconds per band, and thus is rather shallow (for example, the r'-band 5 σ limiting magnitude is 22.2 mag). For this reason, in most cases the SDSS can only probe the normal galaxy population up to $z \approx 0.4$. However, the Stripe 82 region, which is a long stripe along the equator that spans $20^h < RA < 4^h$ and $-1.26^o < Dec < 1.26^o$, totalling in ≈ 300 deg^2 is the exception. It was repeatedly scanned ($\sim$ 70-90 times, depending on RA) for calibration purpose during the survey (Adelman-McCarthy et al. 2007), and thus the combined scans can reach much better sensitivities.

A number of teams have created deep Stripe 82 stacks and made them available to public. The first such stacks were produced by Annis et al. (2014) based on the data obtained up to December 2005 (20-35 runs), which achieved 1-2 magnitude deeper limits than the single-pass SDSS images. Several other teams (e.g., Jiang et al. 2009; Huff et al. 2014) produced different stacks using different procedures to optimize the image qualities.

Jiang et al. (2014; hereafter J14) released a new version of stacks using only the images that were taken under the best weather conditions. These stacks are $\sim$ 0.2 mag deeper than those produced by Annis et al. (2014), reaching 5 σ limits of 23.9, 25.1, 24.6, 24.1, 22.8 mag in $u'g'r'i'z'$, respectively, and also have better PSF characteristics. We adopt these stacks in our work.

2.2. *Structure of SDSS Stripe 82 files*

We use description from J14 to present the structure of optical data. An SDSS run (strip) consists of six parallel scanlines, identified by camera columns (Figure **??**). The scanlines are 13.5 arcmin wide, with gaps of roughly the same width, so two interleaving strips make a stripe that consists of total 12 scanlines (columns).

The size of each co-added SDSS image is 2854 x 2048 pixels, or roughly 18.8' x 13.5' (RA x Dec), with a pixel size of $0.396''$ and an average full width at half maximum (FWHM) of $\sim 1.5''$ in u-band, $\sim 1.3''$ in g-band, and $\sim 1''$ in r-, i-, and z-bands. In total there are 401 SDSS images in each column and overall $12 \cdot 401 \cdot 5 = 24,060$ SDSS images in all 5 bands. Each SDSS image has a corresponding weight.fits image, that records relative weights at individual pixels.

2.3. *WISE and unWISE*

WISE (Wright et al. 2010) is a near-to-mid IR space telescope launched in 2009 and has performed an all-sky imaging survey in four bands at 3.4, 4.6, 12, and 22 μm (denoted as W1, W2, W3, and W4, respectively). During its original mission phase from 2010 January 7 to

2010 August 6 (the "4-band Cryogenic" phase), WISE surveyed the entire sky 1.2 times in all four bands simultaneously until the solid hydrogen coolant in the outer cryogen tank was depleted. It then entered the "3-band Cryogenic" phase for the next 54 days, during which time it mapped an additional 30% of the sky in W1, W2 and W3. When the coolant in the inner tank was also depleted by 2010 September, only W1 and W2 are operational. The NEOWISE project took over the mission on 2010 October 1 and brought it into the four-month "Post-Cryo" phase to survey the sky in these two bands for near-earth objects until 2011 February 1 (see Mainzer et al. 2014). The telescope was then put into hibernation for the next 35 months as the funding stopped. The extended NEOWISE project reactivated it in 2013 December to continue the two-band observations ("NEOWISE Reactivation") through today.

The WISE team made three data releases separately for the 4-band Cryogenic, the 3-band Cryogenic and the NEOWISE Post-Cryo phases in 2012 March, 2012 June and 2013 May, respectively. To take the advantage of these repeated observations, the WISE team also made the "AllWISE Data Release" in 2013 November by combining all the WISE data available till then (see Cutri et al. 2013; for details). The included image products, known as the "Atlas Images" reach the nominal 5 σ limits of 0.054, 0.071, 0.73, and 5.0 mJy in the four bands, respectively.

To optimize the detection of isolated sources, the WISE team has been using a special treatment when combining images, namely, the single-exposure images are convolved with the individual point spread function (PSF) during the stacking process. However, this operation has the drawback that it reduces the spatial resolution of the final stacks, which is not desirable in many applications. To deal with this problem, Lang (2014; hereafter L14) reprocessed all the WISE images independently without the PSF convolutions, and produced the stacks that preserve the original WISE spatial resolutions. These image products of L14, dubbed as the "unWISE" images, have the PSF full-width at half maximum (FWHM) values of $6''$ in W1, W2 and W3 and $12''$ in W4. We use these unWISE W1 and W2 images for this work.

2.4. *Structure of unWISE files - once again maybe I need to omit it in the paper*

The unWISE coadds are on the same tile centers as the WISE tiles with 18,240 images per band, 1.56 x 1.56 degrees each. The tiles are named by their RA, Dec center: tile "0591p530" is at RA = 59.1, Dec = +53.0 degrees; i.e., the first four digits of the tile name is $int(RA \cdot 10)$, then "p" for +Dec and "m" for -Dec, then three digits of $int(abs(Dec) \cdot 10)$. For each tile and band W1-w4, several images are produced, we shall list only the ones that we make use of:

– unwise-0000p000-W1-img-m.fits - "Masked" image, 2048 x 2048 pixels, TAN projected at 2.75"/pixel. Background-subtracted, in units of "Vega nanomaggies" per pixel: $mag = -2.5 \cdot (log_{10}(flux) - 9)$. This is the science image, the word "masked" means that some pixels have no unmasked pixels and no measurement at all: pixel value 0 and infinite uncertainty.

– unwise-0000p000-W1-std-m.fits - Sample standard deviation (scatter) of the individual-exposure pixels contributing to this coadd pixel.

Three unWISE images centered at the same RA cover the whole width of Stripe 82 in Dec (-1.26^o to $+1.26^o$). We shall call three such unWISE images a frame. There may be up to 72 SDSS images within one frame.

2.5. *Spectroscopic sample*

Spectroscopic redshifts are used to perform star/galaxy separation and calibrate photometric redshift estimation: determine a set of templates and photometric offsets for the template-fitting code and train machine learning algorithms. We shall call such sample of sources a training set. Originally, we constructed our training set using spectroscopic data from the SDSS DR14 (Bolton et al. (2012)). Spectroscopic redshifts and classification into galaxies, stars and QSOs for the SDSS DR14 catalog are calculated using principal component analysis (PCA). The software idlspec2d is used to perform, at each potential redshift, a least-squares fit to each spectrum, using a fairly general set of models, for galaxies, for stars, for cataclysmic variables, and for quasars. The best fit model and redshift is chosen and assigned for the object.

Their spectroscopic sample consists of a wide variety of galaxies, stars and QSO with no cuts on color, although it is rather limited in terms of redshift (Strauss et al. (2002). Stripe 82 data are 1-2 mag deeper than single-pass images and therefore potentially has a lot of sources at higher redshifts. We decided to extend our training set by cross-matching galaxies in our photometric catalog with spectroscopic measurements of other, publicly available surveys, such as 6dF, WiggleZ, DEEP2, VVDS and VIPERS.

In Tab.1 we list auxiliary catalogs with selection criteria, median redshifts for galaxies and QSO and total number of sources that were added to our training set. For each source, we use published redshift quality flag to select trustworthy sources, but also add stars when possible (which sometimes have special flag or assigned with negative redshift).

We cross-matched the galaxies from the training set with our photometric catalog using 2 asec as maximum separation in RA and Dec.

3. OVERVIEW OF METHODS FOR ANALYSIS

The most critical factor in SED fitting is consistent photometry in the involved bands, i.e., the photometry should include the same fraction of light across all bands so that the colors are defined in a consistent manner. This is challenging in our case because the spatial resolutions of WISE are at least $6\times$ worse than that of the SDSS. For this reason, the objects detected in WISE often suffer blending. Even for relatively isolated WISE sources, the photometric apertures appropriate for the (low resolution) WISE images cannot guarantee the same fraction of light being included as what is done in the (high resolution) SDSS images. Such a systematic offset, which is different for every galaxy, severely skews the SED fitting.

To best address this problem, we opt to use the $\mathtt{T-PHOT}$ software, which recently emerged as a robust and flexible tool to perform "template fitting". The basic idea

Table 1
Spectroscopic training samples.

Survey Name	Selection criteria	References	median redshift	Total number of sources
SDSS DR14	zErr < 0.1; zWarning = 0	Bolton et al. (2012)	0.339	233,123
6dF	Q = 3; 4; 6	Jones et al. (2004), Jones et al. (2009)	0.054	123,135
WiggleZ	23.113231	c	a	a
DEEP2	23.113231	c	a	a
VVDS	23.113231	c	a	a
VIPERS	23.113231	c	a	a

is to use a high-resolution image (here an image from the SDSS) as the prior to build the morphological template of the source under question, convolve this template with the PSF of the low-resolution image (here the corresponding image from the unWISE), and fit this degraded template to the low-resolution image to obtain the total flux that is within the aperture as defined by the high-resolution image. In this way, we get reliable color information (i.e., flux ratio) in the most consistent manner.

While $T - PHOT$ is much more user-friendly as compared to its predecessors, running this software is still non-trivial. It not only requires careful tuning of parameters but also several tedious preparatory steps with both the high- and the low-resolution images. Here we detail our procedures.

3.1. *Initial preparation of unWISE and SDSS images*

T-PHOT requires that the low- and the high-resolution images have the same orientation and the same World Coordinate System (WCS) reference position, the latter of which is defined by the FITS keywords (CRVAL1, CRVAL2). It also requires that their pixel scale ratio must be an integer. To meet these prerequisites, we carried out the following procedures utilizing the SWarp software (Bertin et al. 2002), which can subsample or bin an image to any pixel scale and then re-project to an arbitrary orientation at any tangential point.

We first rescaled the unWISE images from $2.750''$/pix to $2.772''$/pix. As the scale of an SDSS image is $0.396''$/pix, this makes the ratio of their pixel scales an integer $(2.772/0.396 = 7)$. We kept the same orientation, which is always North-up and East-left, and the same reference position for each unWISE image. This process was done for both the W1 and the W2 unWISE images, which are always aligned.

For a given SDSS image, we oriented it to North-up and East-left, and re-projected it at the tangential point as defined by the reference position of the unWISE images that it lies within. In other words, the FITS keywords (CRVAL1, CRVAL2) of the re-projected SDSS image is the same as those of the unWISE images. As an unWISE image covers much larger area and thus encompasses multiple SDSS footprints, the tangential projection point of a reprojected SDSS image is often outside of its coverage. In the extreme cases, it can be as far as 0.7° outside of the image itself.

About 30% of the SDSS images' footprints lie across two adjacent unWISE fields, and therefore need to be treated separately. If an SDSS image has more than 60 arcmin^2 belonging to adjacent unWISE fields, such image is duplicated, and each copy is reprocessed with respect to the appropriate unWISE field as described above. This increases the number of SDSS images from 4,812 to 5,556 per band. All SDSS images in col02 and col11 have $\sim$2.9' overlap with unWISE images centered at Dec=-1.7 and Dec=1.5 respectively. Processing of such small region requires construction of $\sim$930 PSFs per band and 2,000 hours of CPU time and is unviable. This excludes 11.34 deg^2 from the total area for which catalog is constructed.

We note that the above procedures were done for both the science images and the standard deviation (for the unWISE) or the weight (for the SDSS) images. After the subsampling and re-projection, the standard deviation or the weight value per pixel no longer preserves the absolute scale. In other words, the value of a given pixel on an unWISE (SDSS) reprojected standard deviation (weight) image no longer reflects the true standard deviation (weight) on that pixel. Fortunately, this does not affect the performance of T-PHOT, as it only uses these values in a relative sense (i.e., the absolute scale does not matter). However, it will affect the final errors that T-PHOT report, which we will remedy separately (see Section x.x below). (???? We do not do anything with T-PHOT errors!)

We also note that one special treatment needs to be done for the saturated pixels in the unWISE standard deviation images. They are all assigned zero standard deviation in the unWISE release, which is invalid for T-PHOT. We therefore use the `IRAF/imcalc` task to set such values to "9999" before reprocessing.

3.2. *Input SDSS source catalog*

J14 produced object catalogs from their stacked images using `SExtractor` (Bertin & Arnouts 1996). While it is tempting to use them directly as the input source catalogs for T-PHOT on the unWISE images, several caveats prevented us from taking this approach. For examples, these catalogs are not cleaned of duplicated sources from the overlapped areas between adjacent images; they are not matched among the bands and thus have different number of sources for each band; the object detection threshold was set too high and many faint objects were excluded; bright and saturated objects have clusters of false detections; etc. For these reasons, we constructed our own input source catalogs.

3.2.1. *Rationale*

In addition to providing input source information to T-PHOT, our SDSS catalog also provides optical SEDs for all the detected sources. For the latter, it is critical that the colors of a given source are measured consistently across all five bands, or in other words, the photometric aperture of a source must include the same fraction of total light in any given band. To achieve this goal, we took the standard approach by performing "PSF-matching" of the SDSS images. For a given SDSS field, we first matched the size of the PSF in g, r, i, and z-bands (~ 1.0—$1.3''$) to that of u-band, which always has the largest PSF ($\sim 1.5''$; see J14). We then ran matched-aperture photometry using r-band as the reference band, which detects more sources than any other bands. The PSF-matching step was the most tedious part of the process, which required a lot of human intervention. To derive the convolving kernels between two images, we first must obtain the PSFs of both images. As the SDSS PSF varies from image to image, we had to construct it for each image individually. In total, we built 27,780 SDSS PSFs (5,556 per band).

3.2.2. *PSF matching*

An empirical PSF is best derived by combining a large number of bright, isolated point sources (also known as the "PSF stars") distributed over the entire image. The most robust method to derive a PSF is to run the `IRAF` task "psf" interactively on a list of candidate PSF stars and to retain only the best ones in the construction. Given the huge number of images involved, however, this was not practical. After extensive tests, we settled on an approach that would result in reliable PSF stars, which would then allow us to run the "psf" task non-interactively in most cases.

The key in the PSF star selection is to determine whether an object is a point source. Our approach was to compare the "core" magnitude and the total magnitude. The smaller the difference between the two means the more compact the object is. We used SExtractor MAG_APER and MAG_BEST to quantify the core and the total magnitudes, respectively. The size of the aperture depends on the particular band, but in general is $\approx 3.56''$. The second selection involved magnitude cuts (saturated and faint sources were removed) and the use of the stellar classification technique. The later was estimated using SExtractor which uses a neural network as a classifier to assign the values from 0 to 1 to non-stellar and stellar objects to the stellarity parameter CLASS_STAR, respectively. Sources with CLASS_STAR<0.85 were rejected. The last selection only left the source in the final sample if it is not close to the edge of the image and does not have another nearby source within XX''.

Finally, each SDSS image has 20 to 160 point-like sources that contribute to the PSF model. Lower value appears in a few images when there are not enough bright point sources (mostly in the less sensitive u-band), while the cut in the maximum number of the point sources was performed in order to have stable performance of the `IRAF/psf` task. *I know it sounds ugly, but I don't want to write the IRAF sometimes crashes when you supply more than 160 stars.* Visual inspection is given

to all constructed PSFs. If it shows some features, such as elongation, gradient of the background due to the nearby (within up to several arcmin) source, or faint non-detected blended source in the vicinity of the main profile, then manual selection of the point sources and reconstruction of the PSF is performed. `IRAF/seepsf` is used to take the PSF, computed by the `IRAF/psf` and build a 21x21 pixel output FITS image, consisting of the sum of the analytic function and the residual. All PSF images are subsequently normalized to the unity total counts using `wcstools/sumpix` (Mink 1998) and `IRAF/imarith` tasks.

Kernels are constructed by supplying two PSF to the `IRAF/lucy` task that uses algorithm developed by Richardson (1972) and Lucy (1974). Matching to the PSF of the u-band is performed by `IRAF/psfmatch` task that uses $g'r'i'z'$ image and a relevant kernel as an input.

3.2.3. *Optical catalog construction*

Catalogs are produced running `SExtractor` in the dual mode, where r-band matched to u-band ("r matched to u" for short) is used for detection and all five bands (u-band, g matched to u, r matched to u, i matched to u, z matched to u) are consequently used for photometry. Catalogs in each image are then matched by their ID. Original weight images were used for both detection and photometry. As a result, even spurious detections have SNR >5 and real objects have non-realistic associated magnitude errors, which affect the choice of proper templates for SED fitting. This effect is clearly seen on Figure 1 - magnitude errors are plotted against AB magnitudes for all sources from a random image in the g-band. Blue points represent sources from the original g-band image, red points - from the "g matched to u" image. Individual ratio of the magnitude errors per source and than the mean ratio for all the sources was calculated. Right panel of 1 shows such mean ratio for all 5,556 images in the g-band. Black vertical line denotes the ratio of one. Magnitude errors in the "g matched to u" images are considerably underestimated throughout the whole Stripe 82 as compared to the magnitude errors in the original g-band images and this situation persists in all 5 bands. We mitigate such problem by running `SExtractor` in the dual mode again, where

3.3. *Kernels for T-PHOT*

Template fitting requires a kernel - PSF matching function between the high resolution and the low resolution images. We used the same strategy as outlined in the section 3.2.2 and also positions of the PSF sources in r-band to construct PSF in "r matched to u" band which is used as a prior for the unWISE W1 and W2 low resolution images. Due to broader profiles after PSF matching, some PSF sources now have contamination from the neighbor sources. Such PSFs are reconstructed using IRAF/psf in the interactive mode.

Though generally space telescopes have stable PSF due to the absence of the atmosphere variations and PSF models averaged over the focal plane can be used (such approach is used in e.g. D14), we constructed individual PSF for every unWISE image in the Stripe 82 footprint. The reason behind it is that WISE Atlas Images are constructed by co-adding many single-exposure images. Because the number and relative orientation of
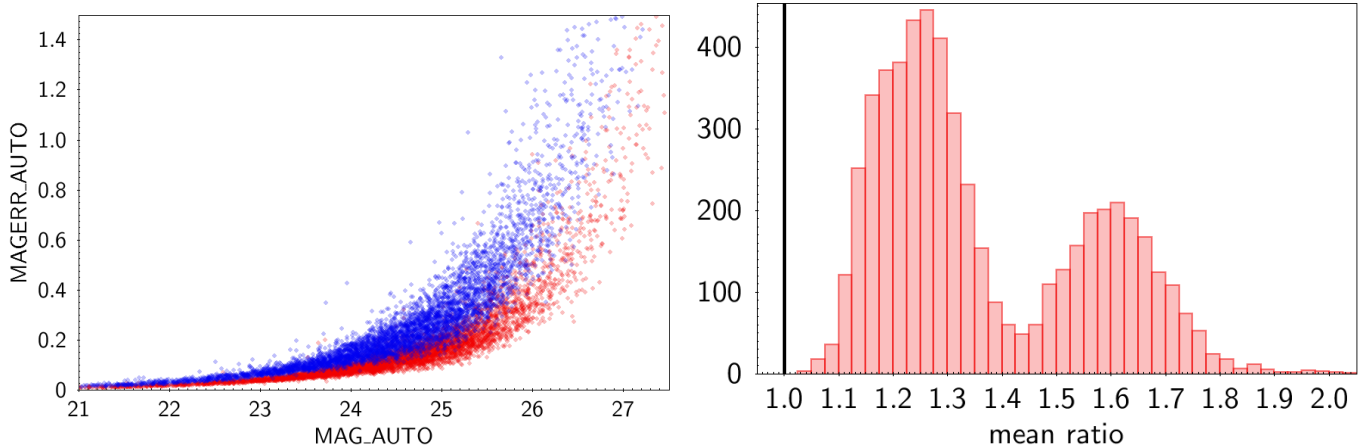
Figure 1. Magnitude error vs. absolute g-band magnitude for one SDSS image. Left panel: magnitude errors in the "g matched to u" image(red) are underestimated as compared to the original SDSS g-band magnitude errors (blue). Right panel: histogram of the mean ratio of the original magnitude errors over magnitude errors in the "g matched to u" image for each of 5,556 images. Black vertical line denotes the mean ratio of 1.

single-exposures differ significantly between Atlas Tiles, and because the single-exposure PSFs vary with focal plane location, the PSF will be different for every Atlas Image and will vary with position on any given Atlas Image. *mostly took it from allsky supplementary materials*

There are 240 unWISE images within Stripe 82 footprint per band. 480 PSFs are constructed in a similar way to the SDSS PSFs with only one change, namely all point-like sources were selected in interactive mode using IRAF/psf. This is done to perform more robust selection of the point sources as 3 PSFs from one unWISE frame are convolved with up to 72 SDSS PSFs and thus its quality is crucial - incorrect PSF profile leads to wrong flux estimation and also creates characteristic positive and negative ring-shaped patterns in the residuals.

All unWISE PSFs are normalized to unity total counts using IRAF/imarith and sub-sampled in size by the factor of 7 using IRAF/imlintran to match the pixel scale ratio between unWISE and SDSS images. IRAF/lucy is used to convolve normalized "r matched to u" PSFs with normalized and sub-sampled unWISE PSFs to create individual kernels.

3.4. *Running T-PHOT*

T-PHOT is a software designed to perform a precision photometry on a low-resolution images using information provided by a high-resolution images of the same field as a prior. Running T-PHOT on such a large portion of the sky with individual kernel for every pair of high- and low-resolution images is a key feature of our project.

Following recommendations from Merlin et al. (2016) two passes are performed on each pair of images. The first pass performs template fitting using provided kernel and also constructs individual kernels for each source on a given image by applying shifts in high-resolution image reference pixels along X and Y directions. These individual kernels are then used in the second T-PHOT pass. Standard pipelines are used for both passes. Single fitting is applied instead of dividing the low-resolution image on a number of individual cells. The former approach requires large amounts of computational time, but it provides the most accurate flux estimate.

One of the advantaged of T-PHOT is a large saving of computational time comparing to its forerunners, TFIT or CONVPHOT codes, but it still needs lots of CPU time. T-PHOT has to be run twice (first pass and second pass) in two unWISE bands, W1 and W2 on each of 5556 SDSS images within Stripe 82. One single pass takes ≈ 3 hours CPU time totaling in 66,700 CPU hours for Stripe 82. Computation is performed on the University of Missouri High-Performance Computing (HPC) cluster Lewis to process all images.

Once all unWISE images within Stripe 82 footprint in W1 and W2 bands are processed by T-PHOT, output catalogs need to be matched with the optical ones. Matching is performed with STILTS code separately for every image using unique source ID as the matching parameter. Due to poorer sensitivity of the WISE as compared to SDSS, 11,367,420 (39%) and 12,868,350 (44%) of sources in bands W1 and W2, respectively were assigned with zero or negative flux. Such sources are kept in the final catalog and are assigned with AB mag = -99 in the corresponding band.

3.5. *Catalog post-processing*

3.5.1. *Star-Galaxy separation*

Our catalog now consists of 29,046,660 objects and is contaminated with stars and QSO that should be removed prior to any SED fitting. There are two major ways to classify stars and galaxies in large sky surveys, namely morphological and photometric separation. Morphological approach separates point-like sources (stars and QSO) from extended using flux profiles, while photometric separation uses rest-frame optical, near-IR (AB W1-W2 $\geqslant$ 0.8 cut proposed in Stern et al. (2012) for the AGN detection) or FIR (Pollo et al. (2010)) colors to isolate regions that are mainly populated by stars or QSO. While the former method has a risk of loosing faint compact galaxies that outnumber halo stars at depth r'>24 AB, we choose to use it as the latter method is not applicable in our case: optical colors cannot be used because star and QSO's loci populate the same space as sources that we classify as galaxies (Figure 2), and W1 and W2 bands cannot be used because only 45% of sources have proper photometry in both near-IR bands.

Morphological classification that we decide to apply is

based on the SExtractor CLASS_STAR parameter that is assigned to each object and is bounded within the stellarity index from "0" (galaxy) to "1" (star). SExtractor uses neural network with the back propagation learning procedure and 10 input parameters: 8 isophotal areas, 1 peak intensity and seeing. Seeing for the given image can be easily estimated as the FWHM of the PSF with IRAF/imexamine and we use the advantage of already constructed PSF for every original (i.e. not matched to the u-band) image in 5 optical bands to find the combination of CLASS_STAR parameters in different bands that shows the best performance in the star-galaxy separation. We use spectroscopically confirmed sample of 254,190 sources classified by the SDSS team (Bolton et al. (2012)) to find the optimum: CLASS_STAR parameters should be simultaneously less than 0.47, 0.43 and 0.75 in bands g'r'i', respectively to have the lowest fraction of missed galaxies (1.76%) and contamination from stars and QSO (2.39%).

Morphological separation of stars/QSOs and galaxies has a risk of misclassification of faint objects that could be compact or distant galaxies. We anticipate that this will not be a major issue: faint galaxies will have isophotes disturbed by the background noise and thus will not appear point-like and distant bright galaxies should not be classified as point sources because average seeing in $g'r'i'$ bands is $\approx 1''$ which corresponds to the maximum angular size of 8.464 kpc at z=1.7 which is well below of the diameter of the normal size galaxy.

After performing star-galaxy separation our catalog contains 15,842,283 galaxies.

3.5.2. *Removing duplicate sources*

Adjacent SDSS images have 25" and 28" wide overlapping regions in RA and Dec, respectively and adjacent unWISE images have 186" and 180" wide overlapping regions regions in RA and Dec, respectively. Sources in these regions appear in the catalog more than once and should be removed. Internal match on the catalog is performed and 1,423,979 duplicate sources with lower SNR in r-band are removed using 1.2 asec matching radius.

3.5.3. *Masking bright regions*

Objects that are extremely bright in near-IR present a number of problems to the photometry measurement of the nearby sources because it generates a host of artifacts. These artifacts include halos (low surface brightness emission extending well beyond the PSF), diffraction spikes, stripes of saturated pixels and residual ghosts. These artifacts will compromise the reliability of W1 and W2 photometry performed by TPHOT. To account for such artifacts the natural solution is to mask certain regions based on available catalogs. We used SAO star catalog Staff (1966) and Bright IR Stars Compilation (BIRSC) [R. Tam and C. Xu - IPAC] as a base for the masking catalog. There are around 400 stars in both catalogs within Stripe 82 footprint, but our visual inspection showed that some very bright objects (both stars and galaxies) that severely alters results of TPHOT are still not in this list. We inspected all residual FITS images and added 300 more objects to the list that now consists of 705 objects. Masking area depends on the provided V-band magnitude if exists and visual estimation of the halo size otherwise. Radii for masking are ranging from

50 to 600 arcsec. An example of such source with 100 asec masking radius is shown on Figure 4.8. The overall masked area is 3.866 deg^2, which reduces the total sky area of the survey to 288.212 deg^2.

4. PHOTOMETRIC REDSHIFT ESTIMATION

There are two main ways to estimating redshifts from broad-band photometry: using machine learning and template fitting approach.

Machine learning uses algorithms to find patterns in a training set on a color-redshift or magnitude-redshift plane. Training set usually consists of the fraction of the catalog sources for which true redshift is known from spectroscopic surveys. Combination of the patterns with corresponding weights is then used to assign photometric redshift to the sources for which spectroscopic redshift is unknown.

Template fitting approach uses a set of spectral templates (either theoretical or empirical) and filter transmission curves to compute synthetic magnitudes at different redshifts and compare it to the observed magnitudes of the source under question. Photometric redshift is then estimated statistically: χ^2-minimisation or Bayesian analysis is used to find the combination of synthetic magnitudes or colors that reproduces observed ones best.

Machine learning codes outperforms template fitting ones within the space that is covered by the training set and are also much faster. Its performance outside of this space is generally poor and what is more important has intrinsic problems with estimation of the accuracy.

There are two factors that reduces the accuracy of redshift estimation and intrinsic to both approaches: color-redshift degeneracy and photometric measurement errors. Color-redshift degeneracy is a well-known physical phenomenon when two galaxies have different stellar populations, sizes, metallicities and redshifts, but share the same position in a magnitude (or color) space. A classic example would be a compact low-redshift galaxy with old stellar population and massive high-redshift galaxy with ongoing star-formation - they both appear to have similar (i.e. red) colors and observed magnitudes. Photometric measurement errors is an even more important issue - they blur the divisions in color space between different galaxy types and similar galaxies but at different redshifts and it becomes even more severe at fainter magnitudes. If photometric measurement errors are systematic in different bands, this problem can be partially solved by applying photometric offsets - we discuss it in Section (XX).

Theoretically, template fitting approach has an important advantage over machine learning one: it does not require training set and thus can be applied in the fields that do not have any spectroscopic data or in the fields where spectroscopic data are not representative for the whole data set (either in terms of the redshift range, colors or magnitudes), since entire set of continuous spectral energy distributions is known. However, the exact choice of computational code, set of templates and a-priori unknown systematics in the photometric measurements that is required to significantly improve the quality of fitting, may only be estimated in a series of tests using a sub-sample with spectroscopic redshifts.
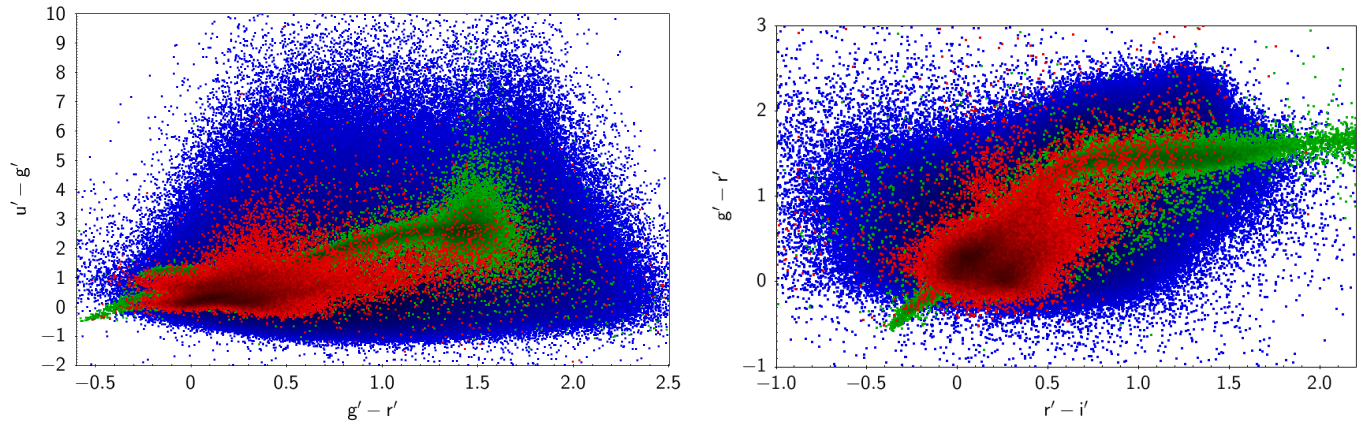
Figure 2. Color-color planes u'g'r' (left) and g'r'i (right) occupied by all sources classified as galaxies (blue) based on morphology are overplotted with stars (green) and QSO (red) that are spectroscopically classified by the SDSS team (Bolton et al. (2012)).
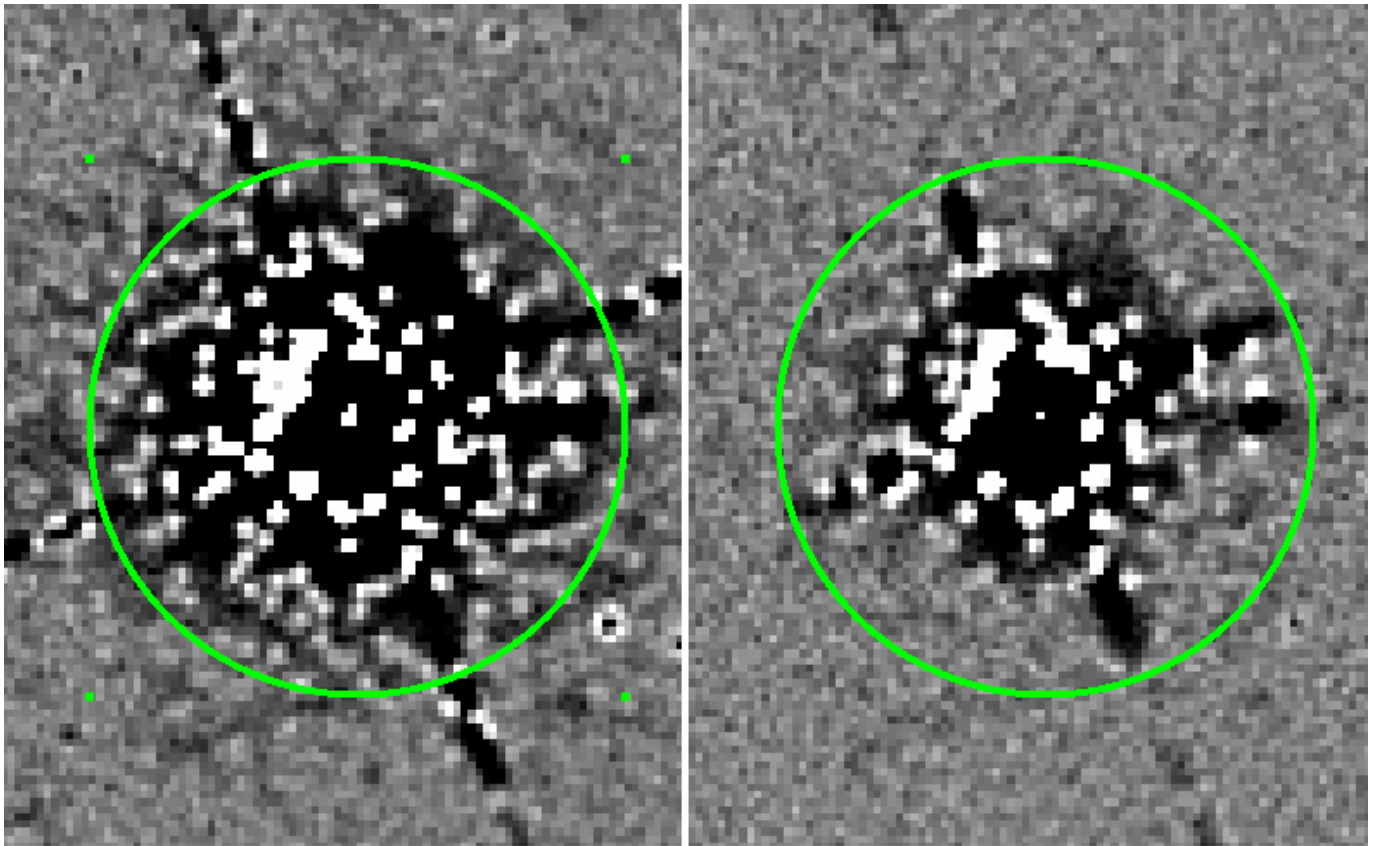

Figure 3. W1 (left) and W2 (right)T-PHOT residuals of the bright star. Area inside a region with a radius 100 asec (green) is masked.

I rewrote till this phrase

The availability of near-IR filters helps improving the z phot accuracy beyond z $\approx$1.3, where the 4000A break goes out of the z-band and the Lyman break is not yet detectable in the u-band. (from 1809.03373.pdf)

comparison of the redshift with and without unWISE data (almost similar results with an exception in the z≈0 and overall scatter)

4.1. *suspicious photometry in W1 and W2 bands*

Outliers in the z-W1 vs W1-W2 plane were assigned with negative fluxes in the WISE bands and it improved fitting in EAZY.

4.2. *combining results of photometric redshifts*

median (as there's no difference as described in Dahlen et al 2013 and also I can't compare odds (from ANNz) and chi2 (from EAZY).

4.3. *Outliers*

Check my notes p8. and section 4.8 of Dahlen et al 2013

Majority of outliers are diifferent for different codes, 1250 of them are outliers in all 4 codes and also outliers in SCUSS, Reis, CFHTLS and SDSS DR15 (which are photo-z catalogs). 460 of them have zWarning=4 from SDSS DR14 (chi-squared of best fit is too close to that of
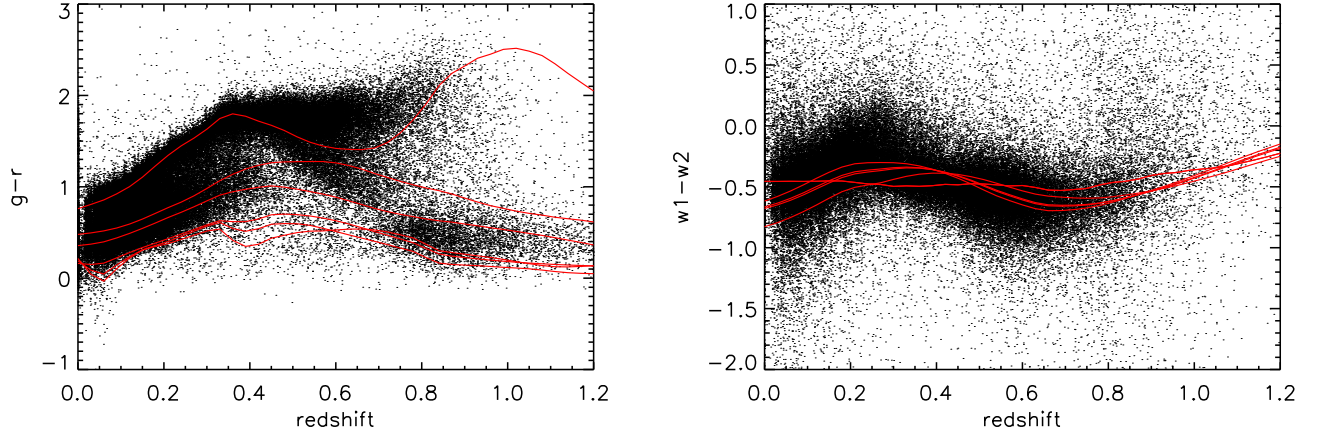
Figure 4. Color vs. spectroscopic redshift for the whole set of the photometric catalog sources (colored black) with available spectra. Colors of the six CWW+KIN templates as a function of redshift templates are plotted as red lines. These templates alone cover sufficient area on the plane and their linear combination returns reliable photometric redshift

second best), so it is not necessary that our photo-z are wrong. So it is possible that the real fraction of outliers is even smaller than reported here.

5. RESULTS

5.1. *testing against available photo-z catalogs*

SCUSS, SDSS DR15, Reis et al, CFHTLS

6. DISCUSSION

7. SUMMARY

REFERENCES

Adelman-McCarthy, J., M.A., A., S.S., A., et al. 2007, VizieR Online Data Catalog, 2276

Annis, J., Soares-Santos, M., Strauss, M. A., et al. 2014, ApJ, 794, 120

Arnouts, S., & Ilbert, O. 2011, LePHARE: Photometric Analysis for Redshift Estimate, Astrophysics Source Code Library, ascl:1108.009

Bertin, E., & Arnouts, S. 1996, A&AS, 117, 393

Bertin, E., Mellier, Y., Radovich, M., et al. 2002, in Astronomical Society of the Pacific Conference Series, Vol. 281, Astronomical Data Analysis Software and Systems XI, ed. D. A. Bohlender, D. Durand, & T. H. Handley, 228

Bolton, A. S., Schlegel, D. J., Aubourg, É., et al. 2012, AJ, 144, 144

Bolzonella, M., Miralles, J.-M., & Pelló, R. 2011, Hyperz: Photometric Redshift Code, Astrophysics Source Code Library, ascl:1108.010

Brammer, G. B., van Dokkum, P. G., & Coppi, P. 2008, ApJ, 686, 1503

Cutri, R. M., Wright, E. L., Conrow, T., et al. 2013, Explanatory Supplement to the AllWISE Data Release Products, Tech. rep.

Huff, E. M., Hirata, C. M., Mandelbaum, R., et al. 2014, MNRAS, 440, 1296

Jiang, L., Fan, X., Bian, F., et al. 2009, AJ, 138, 305

—. 2014, ApJS, 213, 12

Jones, D. H., Saunders, W., Colless, M., et al. 2004, MNRAS, 355, 747

Jones, D. H., Read, M. A., Saunders, W., et al. 2009, MNRAS, 399, 683

Lang, D. 2014, AJ, 147, 108

Lucy, L. B. 1974, AJ, 79, 745

Mainzer, A., Bauer, J., Cutri, R., et al. 2014, in Lunar and Planetary Inst. Technical Report, Vol. 45, Lunar and Planetary Science Conference, 2724

Merlin, E., Bourne, N., Castellano, M., et al. 2016, Astronomy and Astrophysics, 595, A97

Mink, D. J. 1998, in Bulletin of the American Astronomical Society, Vol. 30, AAS/Division of Dynamical Astronomy Meeting, 1144

Pollo, A., Rybka, P., & Takeuchi, T. T. 2010, A&A, 514, A3

Richardson, W. H. 1972, Journal of the Optical Society of America (1917-1983), 62, 55

Staff, S. 1966, Smithsonian publ. 4652

Stern, D., Assef, R. J., Benford, D. J., et al. 2012, ApJ, 753, 30

Strauss, M. A., Weinberg, D. H., Lupton, R. H., et al. 2002, AJ, 124, 1810

Wright, E. L., Eisenhardt, P. R. M., Mainzer, A. K., et al. 2010, AJ, 140, 1868

APPENDIX

APPENDIX

ACKNOWLEDGMENTS